Available online at www.sciencedirect.com

ScienceDirect

Advances in Space Research 69 (2022) 4111–4122

ADVANCES IN SPACE RESEARCH (a COSPAR publication)

www.elsevier.com/locate/asr

Application of independent component analysis to GPS position time series in Yunnan Province, southwest of China

Weijie Tan [a], Danan Dong [a,b], Junping Chen [a,c,*]

[a] Shanghai Astronomical Observatory, Chinese Academy of Sciences, Shanghai 200030, China
[b] Engineering Center of SHMEC for Space Information and GNSS, East China Normal University, Shanghai 200242, China
[c] School of Astronomy and Space Science, University of Chinese Academy of Sciences, Beijing 100049, China

Received 27 August 2021; received in revised form 4 March 2022; accepted 14 March 2022
Available online 18 March 2022

Abstract

Pervasive seasonal signals have been found in GPS site position time series. A critical aspect in the seasonal geodetic analysis is the identification and extraction of different sources of deformations in space and time domains. In this work, we applied the independent component analysis (ICA) to discriminate four different seasonal periods in GPS time series: spatial uniformly distributed annual signals, local annual variations with spatial heterogeneity, spurious signals of draconitic terms, and semiannual terms. The annual displacements could be well described by surface mass loadings. As we successfully identified the draconitic terms, we removed these terms from the GPS time series and re-estimated the annual signals from the GPS; the annual amplitude reduced by ~1 mm on average. Our results show that the GPS draconitic terms bias the annual signal estimation in conventional sinusoidal model fitting and that the ICA can be successfully used to extract different seasonal periods. We recommend removing the draconitic terms before estimating the annual signals, which are intended for high-accuracy applications.

Keywords: Independent component analysis (ICA); GPS draconitic term; Annual variations; Seasonal signals; GPS time series

1. Introduction

The GPS site position time series contain evident seasonal variations, which can be partly explained by mass loadings and thermoelastic deformation. However, some artificial seasonal signals, such as the GPS "draconitic" year, are also present in the GPS time series. The GPS "draconitic" year corresponds to the GPS constellation period with respect to the sun of approximately 351.2 days or a frequency of 1.04 cycle per year (cpy) (Ray et al., 2008; Amiri-Simkooei, 2013; Rodriguez-Solano et al., 2014; Zajdel et al., 2020). A complete separation and unbiased estimation of the annual variations are critical to ensure velocity estimations and a correct interpretation of the investigated geophysical processes. A challenging task is the separation of the annual variation and the draconitic term. The draconitic term has been uncovered in the power spectrum of GPS position residuals (after fitting and removing the linear trends plus seasonal variations) (Ray et al., 2008). Later, the draconitic term was found in various International GPS Service (IGS) products, including station coordinates, satellite orbits, and earth rotation parameters (Griffiths and Ray, 2013; Ray et al., 2013; Rodriguez-Solano et al., 2014; Zajdel et al., 2020).

A power spectrum analysis can only confirm harmonics at multiples of 1.04 cpy in the GPS coordinate time series (Ray et al., 2008). Currently, the sources and temporal patterns of the draconitic errors have not been thoroughly

* Corresponding author at: Shanghai Astronomical Observatory, Chinese Academy of Sciences, Shanghai 200030, China.
E-mail address: junping@shao.ac.cn (J. Chen).

https://doi.org/10.1016/j.asr.2022.03.016
0273-1177/

clarified. In conventional GPS time series analyses, researchers have assumed the draconitic term to be sinusoidal and applied a harmonic analysis to separate it from the annual term (Altamimi et al., 2016; Chanard et al., 2018). A direct estimation of the draconitic term and its multiples along with other conventional terms, however, has two limitations. First, the close frequencies between the GPS draconitic errors and the annual signals require longer time series (approximately 25 years) to ensure complete separation (Ray et al., 2008). Second, the origin of the draconitic term remains unknown; hence, the sinusoidal model may not be optimal.

Altamimi et al. (2016) applied 21-year GPS observations to estimate the impact of draconitic errors on the station velocities and concluded that they would not affect the linear station velocity determination. Chanard et al. (2018) used 10-year GPS observations to apply a sinusoidal model of the draconitic period and derived its harmonic to assess its impact on the annual displacements. They found that estimating and removing the draconitic signals does not improve the fit to observations. However, in reaching the above conclusions, the annual and draconitic variations were assumed to be purely sinusoidal. Are the draconitic variations purely sinusoidal? If not, how can we separate them to obtain their real variation forms? Amiri-Simkooei (2013) applied a multivariate analysis to 10-year GPS observations and showed that the draconitic error has a non-negligible influence on station coordinates, up to ±3.3 mm and ±6.5 mm in the horizontal and vertical components, respectively. This significantly limits the high accuracy applications of GPS products. To solve the apparent conflict, researchers are pursuing more robust methods and strategies to isolate the draconitic variations in the time domain.

The principal component analysis (PCA) and independent component analysis (ICA), which are nonparametric methods, have been used to isolate and extract hidden signals in GPS time series. The PCA decomposition is based on the power of the components, making it ideal when there is a prominent signal in a time series, such as the common mode error (CME) (Dong et al., 2006; Yuan et al., 2018a). However, when there are multiple signals with close frequencies in the time series, the PCA decomposition cannot separate them thoroughly. On the other hand, the ICA approach (Hyvärinen and Oja, 2000; Comon and Jutten, 2010; Gualandi et al., 2016) is based on the statistically independence of the signals and has been successfully applied to extract the signals of mass redistributions (Liu et al., 2015; Larochelle et al., 2018; Yan et al., 2019), nonlinear tectonic slips (Gualandi et al., 2017; 2020), and systematic errors from GPS observations (Ming et al., 2017; Liu et al., 2017, 2018). Gualandi et al. (2020) applied the ICA to separate tectonic deformations and recover the contributions of afterslip and viscoelastic relaxation. Gualandi et al. (2017) obtained an independent component (IC) that explained fault transient slips. Larochelle et al. (2018) successfully extracted the draconitic second harmonic from the coordinate solution series in the Arabian Peninsula area. However, they could not obtain the base tone of the draconic terms. Yan et al. (2019) applied the ICA to separate the different contributions of four mass loading sources in Chinese mainland.

The objective of this study was to discriminate the annual, semiannual, and draconitic terms around a frequency of 1.04 from the GPS seasonal residual series. We first applied the ICA to the GPS coordinate time series of Yunnan Province in China to isolate the annual signals and GPS draconitic errors. Subsequently, we removed the GPS draconitic terms to evaluate their impact on the estimation of the annual signals. Finally, we quantitatively assessed the improvements in the estimation accuracy of the annual signals.

2. Data and method

2.1. GPS coordinate time series

Since 2011, the Crustal Movement Observation Network of China (CMONOC) GNSS network has been fully operational. Since then, the SHA GNSS analysis Center (https://202.127.29.4/shao_gnss_ac/products/) has included the CMONOC network into its routine global GPS network data analysis using the iGPOS (integrated Geodetic Platform of SHAO) software (Chen et al., 2012). Its processing models and strategies are similar to the IGS zero-difference routine data analysis. We incorporated ~70 globally distributed IGS sites along with 260 CMONOC sites in our data processing to simultaneously estimate the Earth's orientation, satellite orbit, site position, and atmospheric delay parameters. The site positions have demonstrated an agreement of approximately 3 mm in the horizontal component and 6 mm in the vertical component compared with the IGS products (Chen et al., 2012). Thus, the solutions of the regional CMONOC stations are considered to be consistent with the IGS framework and reliable to study the regional crustal deformation. We used the daily coordinate time series processed by the SHA analysis center up to December 2018. The daily solutions were realized in the ITRF2008 reference frame.

The Yunnan Province of China (Fig. 1) is characterized by complex tectonic and nontectonic deformations. The distinctive patterns of the seasonally vertical variations in this region have been used to study the geodynamic processes (Hao et al., 2016; Jiang et al., 2017; Yuan et al., 2018b). We selected 22 CMONOC sites in the region (Fig. 1) with data covering from 2011.2 to 2019.0. We applied a trajectory model comprising the offset, trend, annual, and semiannual variation terms, and jumps to fit the time series. Since the regional GPS time series always contains CME, we applied the PCA (Dong et al., 2006; Yuan et al., 2018a) to extract and remove the CME. In this study, we employed the conventional GPS analysis strategy to estimate and remove the annual and semiannual signals

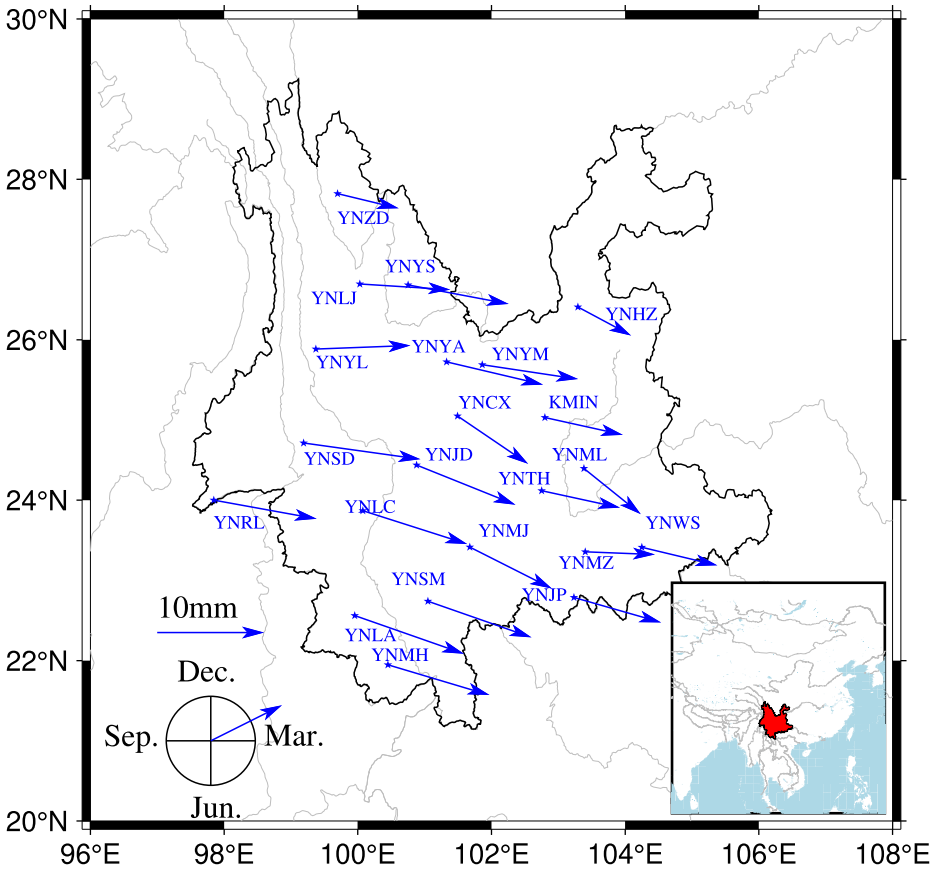

Fig. 1. Annual signals in Yunnan Province of China derived from GPS time series (2011.2–2019.0). The amplitude A and phase ϕ are defined as $Asin[w(t-t_0)+\phi]$, where t_0 is 2000.0, and w is the annual angular frequency. The arrows represent the amplitudes. The phases are counted counterclockwise from the east.

first, then performed regional filtering to remove the CME, and then added back the seasonal signals to generate the seasonal residual time series. We called such residuals the GPS seasonal residuals. Considering the significant annual variations in the vertical, we focused on the vertical annual variations rather than the horizontal annual motions in this work.

2.2. FastICA

The ICA is a computational signal processing method that can decompose the observed mixed signals into statistically independent components (ICs) (Comon and Jutten, 2010). For a set of mixed observed signals $X_{m\times l}$ (m is the number of time series, and l is the total number of recorded epochs) with n unknown zero-mean and statistically independent components $S_{n\times l}$, the two can be expressed as a linear relationship:

$$X_{m\times 1} = A_{m\times n}S_{n\times 1} \quad (1)$$

where $A_{m\times n}$ is a nonsingular mixing matrix. If we estimate the matrix A, we can compute its inverse and obtain the independent components. In practice, we cannot determine such an inverse matrix exactly, because we have no knowledge of matrix A; however, we can find an estimator that gives a good approximation. In the ICA, it assumes that the basic source components $S_{n\times l}$ are statistically independent from each other and that all the source signals (expect, at most, one) have non-Gaussian probability distributions (Hyvärinen and Oja, 2000). The broadest definition for the independence of the ICA is the maximization of non-Gaussianity. We must find an un-mixing matrix $B_{n\times m}$ to obtain $Y_{n\times l}$, which maximizes Y to be non-Gaussianity. This can be summarized as follows:

$$Y_{n\times 1} = B_{n\times m}X_{m\times 1} = B_{n\times m}A_{m\times n}S_{n\times 1} \quad (2)$$

If $B_{n\times m}$ $A_{m\times n}$ is close to an identity matrix, and Y can become the optimal approximation to the original source S.

In this work, we assumed that the source signals are temporally independent and applied the FastICA algorithm (Hyvärinen and Oja, 2000) to perform the decomposition. The FastICA algorithm measures the non-Gaussianity using approximations to negentropy. It achieves source separation by seeking an orthogonal rotation of preconditioning the whitened observations, which maximizes a measure of the non-Gaussianity of the rotated components. The algorithm is based on a fixed-point iteration scheme for maximizing the negentropy. In addition, the preprocessing steps of the algorithm are centering,

whitening, and dimension reduction of the observations, so that the mixing observed matrix is orthogonal (Liu et al., 2018; Hyvärinen and Oja, 2000). The data centering is achieved by subtracting the mean of each column of the observation matrix $X_{m\times 1}$. The mixed signals are then transformed linearly to be expressed in terms of uncorrelated variables with a variance equal to 1 (whitening).

The FastICA approach has been successfully applied to the decomposition of geodetic data for studies on the CME (Ming et al., 2017; Liu et al., 2018), seasonal variations (Yan et al., 2019), and regional tectonics (Ebmeier, 2016). Ming et al. (2017) calculated the Kurtosis (kurt) of the CMONOC coordinate time series and concluded that the residual time series of CMONOC have non-Gaussianity distributions that cannot be fully described by second-order statistics. In the following sections, we use the FastICA to perform the calculations.

3. Sensitivity tests

To verify the reliability of the ICA decomposition for seasonal signals and systematic errors of GPS data, we performed simulation tests. We simulated 50 different daily time series containing the annual/semiannual signals and the variations in the harmonics at 1.04 cpy. Since the true signal is amplitude modulated, we also added an amplitude variation term in the simulated time series. Subsequently, we mainly focused on seasonal variations with different frequencies. Here, we followed previous studies (Zhang et al., 1997; Mao et al., 1999; Li et al., 2012; Chen et al., 2013) and adopted a noise model comprising white noise and flick noise. Therefore, the modeled time-variable station motion $s(t_i)$ can be written in the form of.

$$\begin{aligned} S(t_i) = {} & a\hat{\mathrm{A}}\cdot sin(2\pi t_i) + b\hat{\mathrm{A}}\cdot cos(2\pi t_i) + c(t_i)\hat{\mathrm{A}} \\ & \cdot \sin(2\pi t_i) + c(t_i)\hat{\mathrm{A}}\cdot\cos(2\pi t_i) + d\hat{\mathrm{A}}\cdot sin(4\pi t_i) \\ & + e\hat{\mathrm{A}}\cdot cos(4\pi t_i) + f(t_i)\hat{\mathrm{A}}\cdot\sin(4\pi t_i) + f(t_i)\hat{\mathrm{A}} \\ & \cdot\cos(4\pi t_i) + g\hat{\mathrm{A}}\cdot sin\left(1.04\hat{\mathrm{A}}\cdot 2\pi t_i\right) + h\hat{\mathrm{A}} \\ & \cdot cos\left(1.04\hat{\mathrm{A}}\cdot 2\pi t_i\right) + j(t_i)\hat{\mathrm{A}}\cdot sin\left(1.04\hat{\mathrm{A}}\cdot 2\pi t_i\right) \\ & + j(t_i)\hat{\mathrm{A}}\cdot cos(1.04\hat{\mathrm{A}}\cdot 2\pi t_i) + \varepsilon(t_i) \end{aligned} \tag{3}$$

where a, b, d, e, g, and h are constant time-averaged wave amplitudes, and $c(t_i)$, $f(t_i)$, and $j(t_i)$ are amplitude variations, written as $e^{0.3\sin(t_i)}$. The simulated constant amplitudes vary in the range of 5–10 mm for annual signals (a, b), 1–5 mm for semiannual signals (d, e), and 2–4 mm for time series at a seasonal tone of 1.04 cpy (g, h). Meanwhile, a noise series $\varepsilon(t_i)$ is overlaid onto each series. Since we only have 8-year GPS observations, we performed 8-year observations with 2923 epochs of the daily GPS station variations. Fig. 2 shows examples of the simulated series.

Following the method presented in Sections 2.2, the ICA decomposes the simulated data into four temporal modes, as shown in Fig. 3. To make the comparison more intuitive, we divided each eigenvector by its maximum (absolute value) elements, so that the response of this "maximum" element is always 100%, and all the spatial response values are in the range (−100%, 100%). We call such an eigenvector a normalized eigenvector. We multiplied the corresponding independent component by the normalization factor. Such an independent component is referred to as a scaled IC. Fig. 3a shows the scaled IC. Fig. 3b shows the normalized eigenvalues. A Lomb–Scargle periodogram (Press et al., 2001) was computed for each normalized IC, as shown in Fig. 3c. The vertical lines are plotted for harmonics of 1.00, 2.00, and 1.04 cpy as an aid.

For the 8-year time series, the ICA can identify the annual, semiannual, and draconitic terms but with slight frequency biases (1.007, 1.999, and 1.034 cpy, respectively). Moreover, the fourth IC (IC4) shows peaks at around 0.937 and 2.000 cpy. Because the ICA performs blind decomposition without any a priori knowledge of the spatiotemporal variations in the source signals, for short-time spans, the non-uniqueness problem of the decomposition becomes pronounced. As the spectral power is significantly lower than the annual, semiannual and draconitic terms, we mainly treat IC4 as errors. In particular, when the time span is shorter than one modulation period, we are inclined to consider the amplitude modulation as amplitude-varying harmonics. To verify this, we performed ten thousand simulation tests with different priori un-mixing matrices for the 8-year span. The results showed slightly diversified decompositions, and the mean frequencies of the ten thousand results were 0.986, 1.999, and 1.032 cpy. We take the difference between the mean value of the recovered frequencies and the simulated frequency, 0.014, 0.001, and 0.008 cpy, as the uncertainties in the annual, semiannual, and draconitic terms, in good agreement with Ray's results (Ray et al., 2008), which showed that the uncertainty in the draconitic term frequency is 0.008 cpy. In conclusion, the ICA can isolate the annual and draconitic signals.

4. Results

4.1. ICs derived from ICA of GPS time series

We applied the FastICA to the GPS seasonal residuals in Yunnan Province to extract the annual signals and GPS draconitic errors. In this work, we determined the number of ICs based on the number of the known seasonal variations in the GPS time series. We mainly considered the annual and semiannual signals induced by mass loadings, seasonal variations in the draconitic terms, and errors in the GPS time series as a priori information to decompose four independent components. The FastICA first imposes the PCA to realize dimension reduction. Since we focus on four ICs, we should obtain at least four principal components (PCs) during the calculation. Furthermore, the ratio for each of the rest of the PCs is less than 3%. To reduce some unknown errors in the GPS time series, we only select the first four PCs that explain 73.59% of the

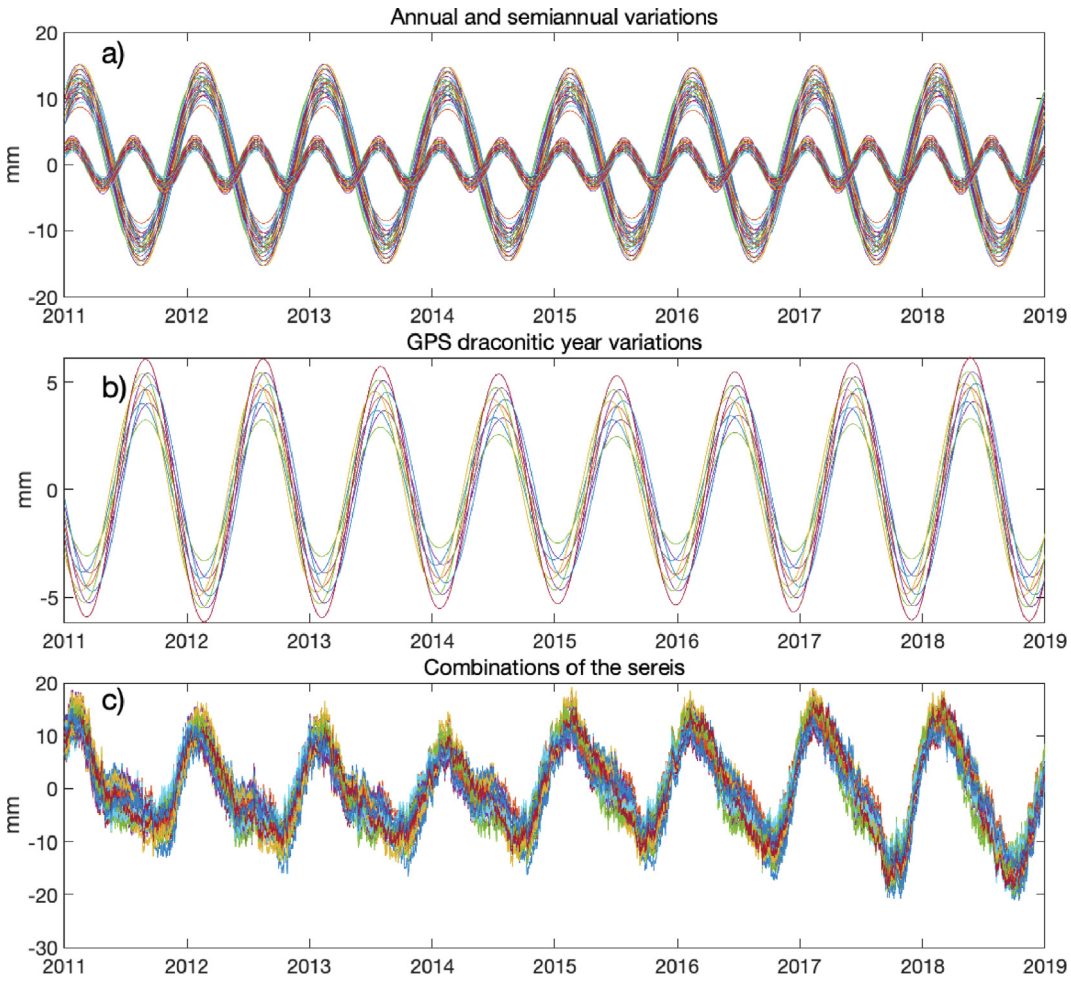

Fig. 2. Examples of 8-year simulated GPS site positions time series data containing modulated amplitude annual, semiannual time series, time variations at a harmonic of 1.04 cpy, and noise. (a) Modulated annual and semiannual variations. (b) Time series at 1.04 cpy. (c) Combinations of the three seasonal variations and noise.

data variance in the seasonal residual data to make the decomposition. Using the composed time series from the four principal components, we recovered four independent components with the ICA. To describe the contributions of the four extracted ICs to the original GPS time series, we adopted the ratios defined by Liu et al. (2018) to depict the effects and reorder the ICs during the calculations. Figs. 4 and 5 show the temporal functions of the extracted ICs and their spatial responses. To verify the seasonal variations for each derived IC, a Lomb–Scargle periodogram was plotted for the four ICs (Fig. 6). The vertical dashed lines are plotted at peak harmonics for each IC: 1.000, 1.032, and 2.001 cpy as an aid.

The ICA decomposition generates two annual components (Fig. 6a and c), where significant seasonal variations are visible in the time domain for IC1 and IC3 (Fig. 4a and c). IC1 demonstrates strong annual variations (Fig. 4a) with nearly uniform spatial responses (Fig. 5a), and its average normalized response is ~68%. IC3 also shows the annual variation pattern but its amplitude is approximately 14% of the amplitude of IC1. Furthermore, the annual phase of IC3 is nearly orthogonal to that of IC1 (Fig. 7a), and the spatial responses of IC3 show small positive responses (except for YNYL, which was affected by groundwater pumping in the past years) in the northwest region and large negative responses in the southeast region of Yunnan Province (Fig. 5c). Such spatiotemporal patterns indicate that the geophysical mechanism of IC3 is likely different from that of IC1. The IC1 represents the annual variations in the dominant geophysical mechanisms with a long wavelength, whereas IC3 likely represents other geophysical mechanisms with spatial heterogeneity.

For IC2, a spectrum analysis shows a peak at 1.032 cpy (Fig. 6b). Over 77% of the sites have significant normalized responses for IC2. It is within the uncertainty range (0.008 cpy for the short time span) of the draconitic frequency (1.04 cpy). Thus, we considered IC2 as the recovered draconitic variations in the GPS time series. There is a small spectrum peak at a frequency of 1.969 (Fig. 6b). Although the peak is close to the semiannual variation, we can also see another peak at around 0.5 cpy. We mainly attribute these peaks to some unknown errors in the GPS time series.

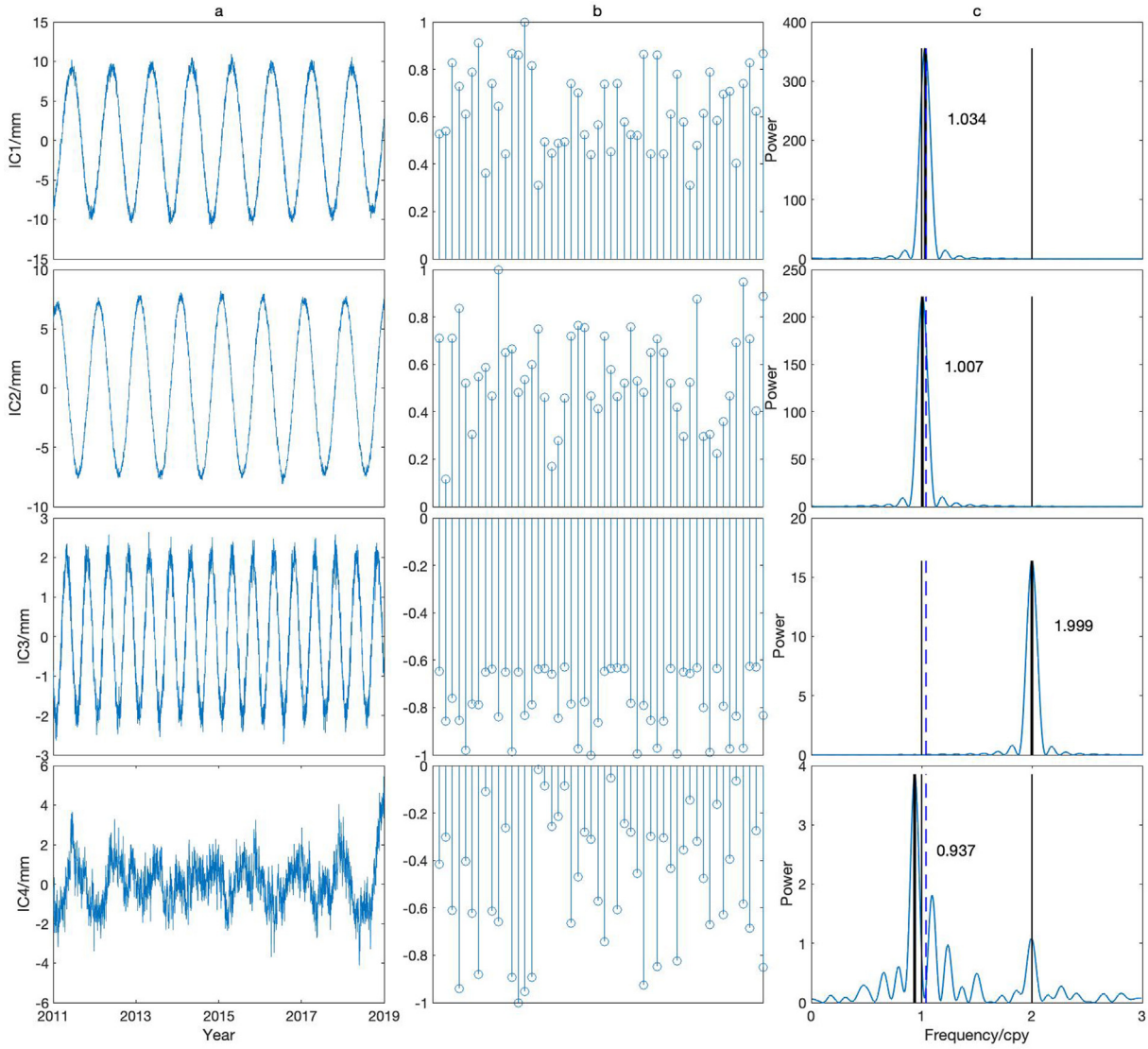

Fig. 3. Recovered source data from ICA for the simulated 8-year GPS time series. (a) Time variations of the four scaled ICs. (b) Eigenvalue of normalized ICs in each index, which we also treat as the spatial responses of each station. (c) Spectra of IC time series. The vertical lines are plotted for the harmonics of the largest and sharpest peaks in each spectrum. The vertical dashed lines are plotted for harmonics of 1.00, 2.00, and 1.04 cpy as an aid.

In additions, evident site variations can be observed during 2017 (Fig. 4b), probably due to the heavy rainfall during the second half of 2017 (Jiang et al., 2021), which aggravated land subsidence in this year. The semiannual variations are mostly in the IC4. Since this study focused on the annual and draconitic terms, we will analyze the semiannual term in a future study.

4.2. Annual signals for IC1 and IC3 (1.00 cpy)

To investigate the mechanisms of the annual signals, we compared the two derived annual ICs with mass loadings from two main sources (surface atmospheric pressure and soil moisture variations). The other mechanisms, such as the nontidal ocean loading, snow, and thermal expansion, can also cause annual deformation. However, their effect induces a deformation of less than 0.5 mm in Yunnan Province (Tan et al., 2017, 2020). Thus, we did not consider the contributions from the thermal expansion, nontidal oceanic effect, and snow mass loading in this study. We first used the atmospheric and soil mass loading models to calculate the mass loading-induced seasonal deformation. The six-hour sampled National Center for Environmental Prediction (NCEP) reanalysis surface atmospheric pressure data from 2011 to 2019 were used to calculate the displacements at each site in the study. The daily sampled GLDAS Noah Land Surface Model L4 (version 2.1, 0.25° × 0.25°, Rodell et al., 2004) was used to calculate the soil moisture mass loading-induced seasonal deformation. The mass loading induced site displacements were calculated using the elastic Green's function approach proposed by Farrell (1972). We also applied sinusoidal fits to obtain the annual variations in the two mass loading modeled deformations, IC1 and IC3, in Yunnan Province.

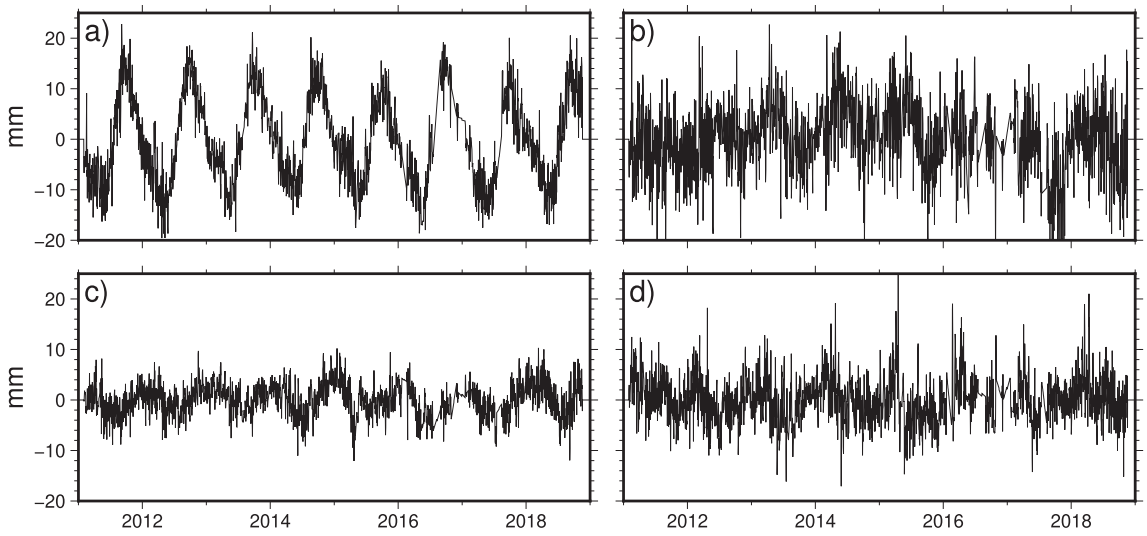

Fig. 4. Temporal variations in the four ICs derived from GPS time series in Yunnan Province by FastICA. (a), (b), (c), (d) IC1, IC2, IC3, and IC4, respectively.

The soil moisture and atmospheric mass loadings are two essential contributors to the seasonal crustal deformation in Yunnan (Hao et al., 2016; Zhan et al., 2017; Jiang et al., 2017; Yuan et al., 2018a; Jiang et al., 2021). The soil moisture induced deformations show long wavelength variation pattern with amplitudes decreasing from southeast to northwest from 7.53 mm to 3.56 mm with a mean value of ~6.34 mm and phases increasing from 1 to 4 days (Fig. 7a). Atmospheric loading induced deformations show nearly uniform patterns with displacements in the range of approximately 2.10–2.85 mm in Yunnan (Fig. 7a). The atmospheric loading induced deformation phases are nearly orthogonal to that induced by soil moisture loadings. Thus, there are two possible explanations for the ICA decomposition. The first one considers that the IC1 represents the contribution from the soil moisture, and the IC3 represents the atmospheric contribution (Fig. 7a) (Yan et al., 2019). Such an explanation has two drawbacks. One is that there are systematic phase deviations between IC1 and soil moisture patterns. The other one is that the IC3 patterns show both positive and negative spatial distributions, while the atmospheric patterns show homogeneous spatial distributions. For a small region, such as the Yunnan Province, both the soil moisture and atmosphere patterns show nearly uniform distributions in terms of their amplitudes and phases (Fig. 7a). Their combination patterns show nearly uniform amplitudes and phases with small perturbations (Fig. 7b).

We adopt the second explanation that the IC1 likely represents the average effects of the joint patterns from soil moisture and atmospheric-induced annual surface deformations (Fig. 7b). The mean phase difference (absolute value) between IC1 and soil moisture + atmosphere loadings (Fig. 7b) is seven days, while the mean phase difference (absolute value) between IC1 and soil moisture loadings (Fig. 7a) is nine days. The comparisons show that the phase differences between IC1 and soil moisture + atmosphere loadings are lower. Moreover, the phase agreements between IC1 and the two mass loadings are better than the phase differences between IC1 + IC3 and soil moisture + atmosphere loadings in most sites (Fig. 7b). This indicates that the differences between joint mass loading patterns and IC1 patterns are likely absorbed by the IC3, whose phases are nearly orthogonal to the phases of IC1. The annual amplitudes of IC1-derived deformations range from 4.71 to 10.75 mm, with a mean value of ~7.42 mm. The IC3 annual amplitude varies from 0.03 to 2.45 mm. In part of the sites, particularly in the northwestern region, the agreements are poor (Fig. 7b). This means that IC3 does absorb the differences in the soil moisture + atmospheric loadings from their averages. However, it may also contain other local effects such as mass loadings from the surface and underground water.

4.3. Draconitic terms (1.04 cpy)

Given the close frequency with the annual signals (1.00 cpy) and the limited data span, we can barely obtain the time series at the harmonic of 1.04 cpy. We typically identify such periodic signals through a spectrum analysis, which shows that peaks are evident at N*1.04 cpy, such as the sharpest and largest peak at 6.24 cpy (Ray et al., 2008). In this study, we estimated and removed the CME in the seasonal residual time series, which also removed the multiples of the draconitic term. If such a seasonal residual time series still contains the harmonics at 1.04 cpy, this not only verifies the existence of the draconitic term, but also reveals that the conventional analysis of the sinusoidal fits of the annual and semiannual terms absorbs the draconitic errors. Hence, the draconitic effects must be considered in the sinusoidal analysis.

By applying the ICA method, close harmonic signals having a period of 351.4 days could be identified in this study. We not only obtain the temporal variations in the

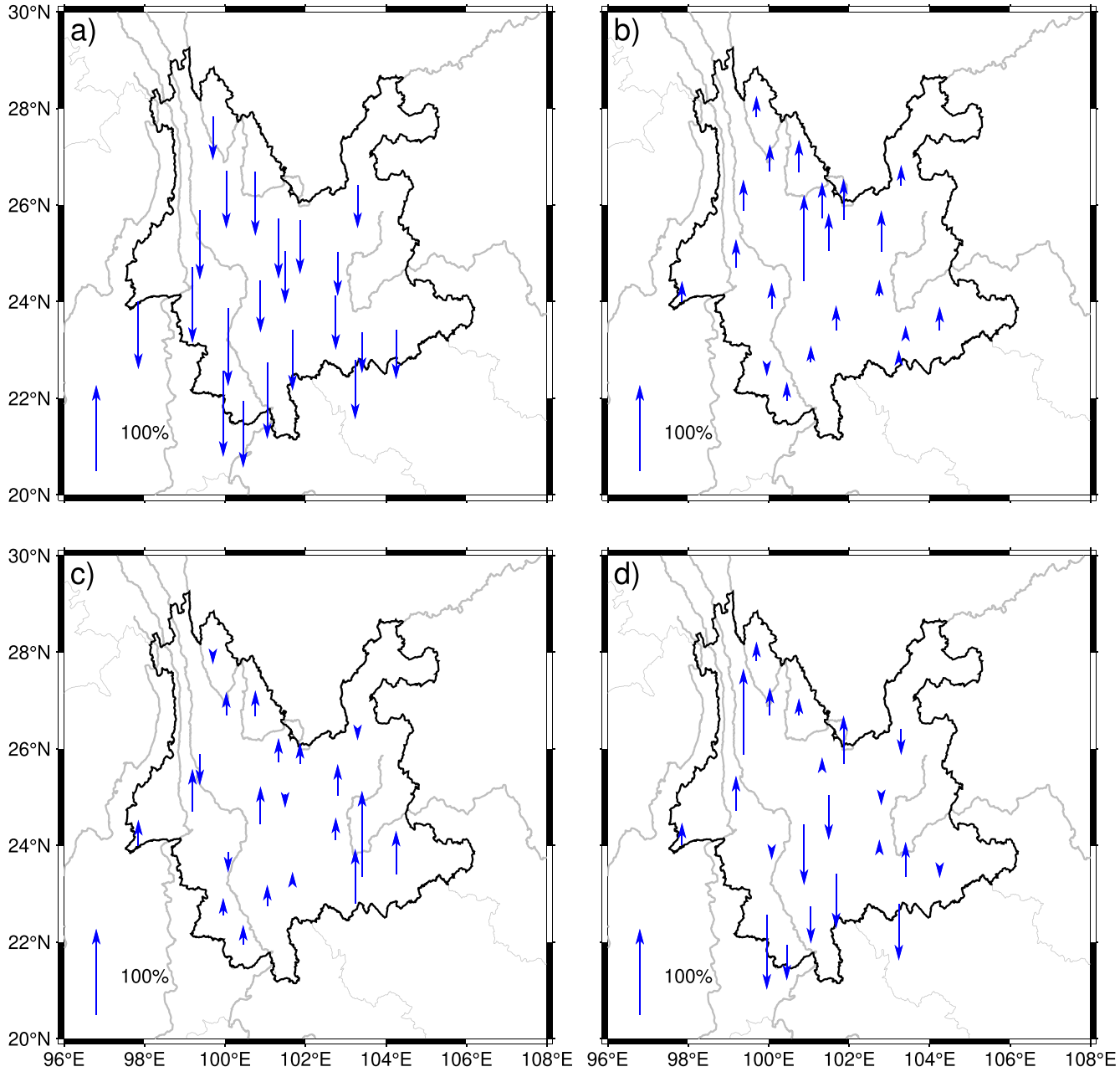

Fig. 5. Spatial responses of the time series shown in Fig. 5. (a), (b), (c), and (d). Spatial responses for IC1, IC2, IC3, and IC4, respectively.

draconitic basic tone, but also show its spatial distributions in Yunnan Province. The mean range (average of all minima and maxima over all GPS stations) of the draconitic terms reaches −10.5–8.2 mm in Yunnan Province. The draconitic amplitude in the region is slightly higher than the global mean amplitude of the draconitic, approximately −6.3–6.7 mm (Amiri-Simkooei, 2013). In this study, we treated IC2 as the draconitic terms and focused on the temporal-spatial variations and their effects on the GPS analysis.

As we successfully isolated the draconitic terms from the true GPS seasonal residual, this is expected to measure their impact on the estimation of annual signals. Using the GPS daily solutions, we estimated the annual signals when the GPS draconitic were removed (Fig. 8, blue arrows). After the draconitic correction in the GPS time series, the annual amplitude reduced in all the sites; however, the annual phase remained almost the same as that of the original GPS in most of the sites. Table 1 shows a quantitative comparison of the annual amplitude and phase with and without the corrections of the draconitic errors. We found that removing the variations at a harmonic of 1.04 cpy reduces the mean annual amplitude to ∼7.55 mm, compared with conventional direct sinusoidal

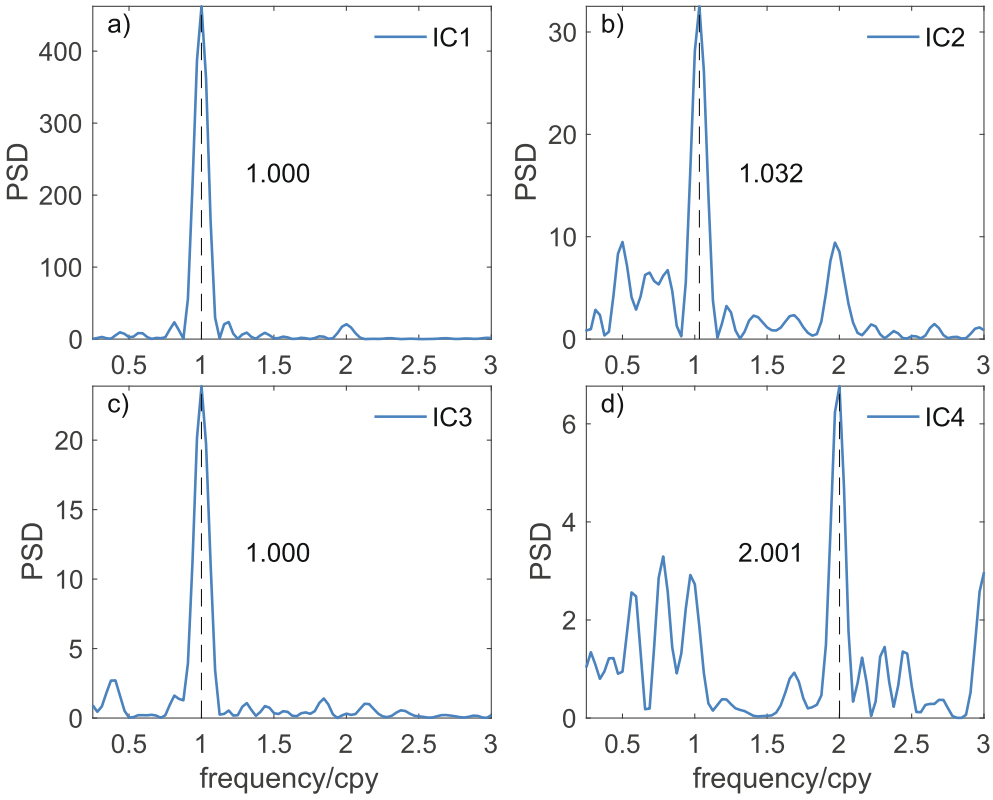

Fig. 6. Power spectra of the four recovered ICs. (a), (b), (c), (d) are IC1, IC2, IC3, and IC4, respectively.

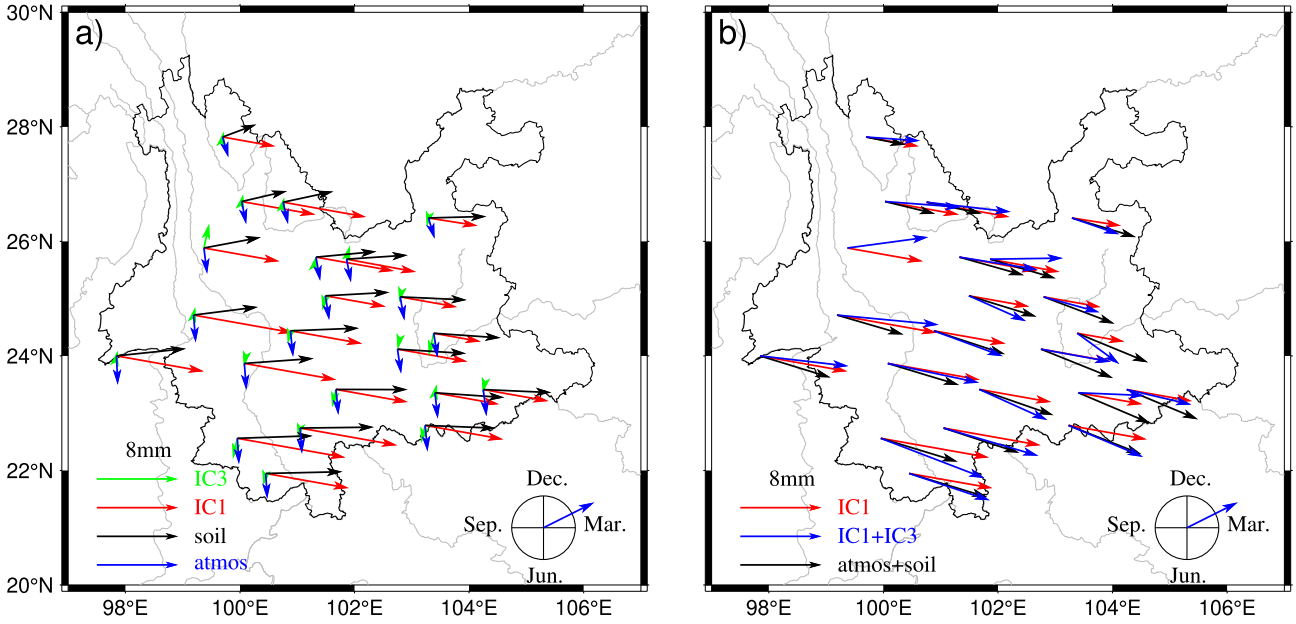

Fig. 7. (a) Annual signals derived from IC1 (red arrows), IC3 (green arrows), soil moisture loading (black arrows), and atmospheric loadings (blue arrows). (b) Annual signals derived from IC1 (red arrows), two mass loadings (black arrows), and IC1 plus IC3 (blue arrows). The amplitude and phase are the same as those defined in Fig. 1.

fitting from the original GPS with an average annual amplitude of ~8.60 mm. The largest annual difference can reach 2.7 mm. The annual power reduces by ~88% when the mass loadings are corrected in the GPS (Table 2). While the GPS draconitic year variations are also estimated, the mass loadings explain 91% of the GPS-observed annual signals.

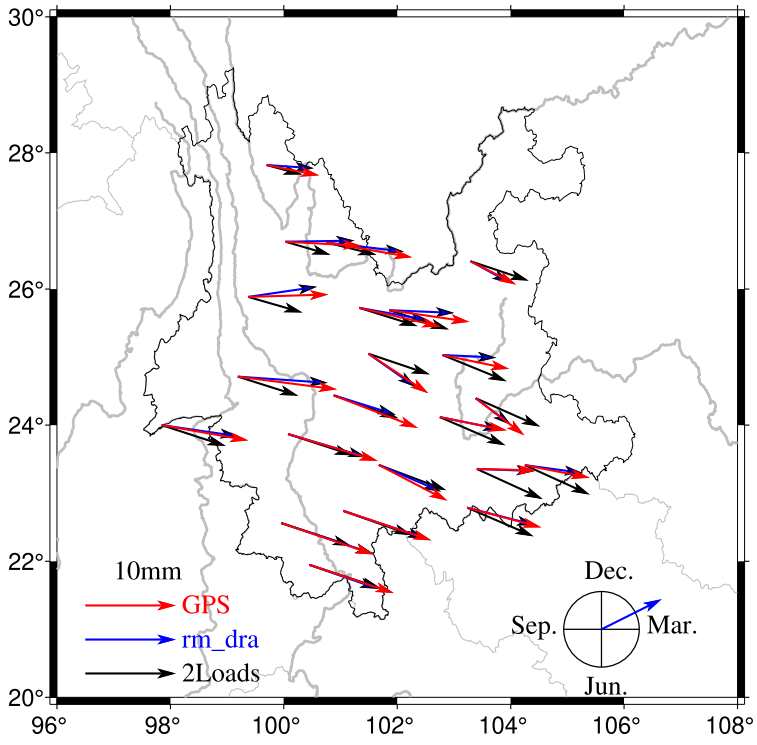

Fig. 8. Annual signals derived from GPS (red arrows), seasonal residual after removing draconitic terms (blue arrows), and two mass loadings (black arrows). The amplitude and phase are the same as those defined in Fig. 1.

Both the annual signals derived from IC1 and time series with draconitic corrections have no draconitic effects. The phase difference between the two signals and the mass loading signals indicates that the GPS time series contains potential seasonal processes or errors. This requires a further study. The annual signals after removing the draconitic terms demonstrate that the draconitic terms will not bias the annual phase of the GPS and have almost ~1.1 mm amplitude effects for the GPS annual amplitude. Given the evident effects of GPS draconitic year errors on annual estimations, we recommend considering the GPS draconitic seasonal effects when focusing on the annual geophysical effects.

Table 1
Annual amplitude and phase of each site before and after the removal of seasonal variations at a harmonic of 1.04 cpy.

Site	Without correction		After correction	
Annual signal	Amplitude (mm)	phase (°)	Amplitude (mm)	phase (°)
KMIN	7.53	348.24	6.82	359.11
YNCX	7.93	326.46	6.62	331.14
YNHZ	5.67	332.91	4.68	338.82
YNJD	9.96	338.82	8.97	343.82
YNJP	8.49	345.18	6.45	2.08
YNLA	10.79	341.25	9.36	348.86
YNLC	10.31	343.37	9.17	346.90
YNLJ	8.43	356.86	8.13	1.14
YNMH	9.84	341.44	7.50	348.42
YNMJ	8.56	332.40	6.78	346.67
YNML	6.79	322.70	4.64	333.98
YNMZ	6.55	358.58	6.00	4.80
YNRL	9.72	349.98	8.22	359.89
YNSD	11.03	352.62	10.32	357.78
YNSM	10.27	341.47	8.90	347.70
YNTH	7.55	348.81	6.75	353.80
YNWS	7.32	348.94	6.44	358.93
YNYA	9.22	346.96	8.64	351.16
YNYL	8.86	1.73	8.22	11.08
YNYM	8.93	351.75	8.61	352.21
YNYS	9.61	350.21	9.23	353.37
YNZD	5.92	348.80	5.63	356.76
mean	8.60	344.97	7.55	335.83

5. Discussions and conclusions

In this work, we recovered four ICs to obtain four different seasonal variations. Researchers have also employed different numbers of independent components for different purposes, e.g., six ICs to recover different seasonal sources (Yan et al., 2019; Liu et al., 2017; Ming et al., 2017), 2 ICs

Table 2
Mean annual amplitude and power explained.

	U
Mean amplitude from GPS	8.60 mm
Mean amplitude after draconitic year correction	7.54 mm
Mean amplitude after mass loading correction	2.54 mm
Power explained (draconitic year and mass loading)[a]	91%
Power explained (mass loading only)[a]	88%

[a] Power reductions: $1 - (A_2/A_1)^2$, where A_1 is the mean amplitude before corrections, and A_2 is the mean amplitude after corrections.

to extract annual signals (Larochelle et al., 2018), and 12 ICs to study post-seismic sources (Gualandi et al., 2020). The decomposed ICs might appear in pairs. When we tried to obtain 8 or 12 ICs in our study, we successfully extracted mathematically independent components of different periods, and these components often appeared in pairs. For example, we obtained two ICs at a frequency of 1.00 cpy, two ICs at a frequency of 1.04 cpy, and two ICs at a frequency of 2.00 cpy. Therefore, the ICA may decompose signals with the same frequency into two mathematically independent signals. Thus, we suggest the number of ICs to be the minimum number of expected signals in the calculations.

We demonstrated that the ICA can help discriminate the annual signals at a harmonic of 1.00 cpy from the draconitic year at 1.04 cpy. Precisely estimating and isolating the GPS draconitic year errors from the GPS site time series are the main results. The GPS draconitic is not only a typical harmonic wave but has its own characteristics in the time domain. It provides direct evidence for studying the regional distributions in the draconitic errors. In addition, the mass loading model-derived seasonal signals were used to validate the origin of the annual signals. In Yunnan Province, the mass loadings explain ~88% of the annual signals in the conventional GPS analysis. After correcting for the draconitic year variations, the mass loadings explain 91% of the annual signals, which provide important clues for the contribution of the annual signals. The seasonal effects of the GPS draconitic year are typically absorbed by the sinusoidal fitting in recent GPS data analyses, thereby overestimating the annual signals from the GPS observations.

The potential impact of the GPS draconitic term on future IGS products seems to be critical in terms of processing strategies in IGS products. The system-specific systematic error in earth rotation parameters can also be used in the application of the ICA method to extract artificial seasonal signals. In addition, we can extract system-specific systematic errors in GPS coordinate time series derived from different GPS systems for a complete understanding of the GPS draconitic year variations.

Declaration of Competing Interest

The authors declare that they have no known competing financial interests or personal relationships that could have appeared to influence the work reported in this paper.

Acknowledgements

This research was funded by National Natural Science Foundation of China (Grant No. 11803065 and 11803032), Natural Science Foundation of Shanghai (Grant No. 22ZR1472800).

References

Amiri-Simkooei, A.R., 2013. On the nature of GPS draconitic year periodic pattern in multivariate position time series. J. Geophys. Res.: Solid Earth 118 (5), 2500–2511. https://doi.org/10.1002/jgrb.50199.

Altamimi, Z., Rebischung, P., Métivier, L., et al., 2016. ITRF2014: A new release of the International Terrestrial Reference Frame modeling nonlinear station motions. J. Geophys. Res.: Solid Earth 121 (8), 6109–6131.

Chanard, K., Fleitout, L., Calais, E., et al., 2018. Toward a global horizontal and vertical elastic load deformation model derived from GRACE and GNSS station position time series. J. Geophys. Res. Solid Earth 123 (4), 3225–3237. https://doi.org/10.1002/2017JB015245.

Chen, J., Wu, B., Hu, X., et al., 2012. SHA: the GNSS analysis center at SHAO. In: Proceedings of the 3rd China Satellite Navigation Conference, CSNC 2012, revised selected papers. Lecture Notes in Electrical Engineering, vol. 160 LNEE, Springer, Berlin, Heidelberg, pp 213–221

Chen, Q., van Dam, T., Sneeuw, N., et al., 2013. Singular spectrum analysis for modeling seasonal signals from GPS time series. J. Geodyn. 72, 25–35. https://doi.org/10.1016/j.jog.2013.05.005.

Comon, P., Jutten, C., 2010. Handbook of Blind Source Separation: Independent component. analysis and applications. Academic press.

Dong, D., Fang, P., Bock, Y., et al., 2006. Spatiotemporal filtering using principal component analysis and Karhunen-Loeve expansion approaches for regional GPS network analysis. J. Geophys. Res. Solid Earth 111 (3), 1–16. https://doi.org/10.1029/2005JB003806.

Ebmeier, S.K., 2016. Application of independent component analysis to multitemporal InSAR data with volcanic case studies. J. Geophys. Res. Solid Earth 121 (12), 8970–8986. https://doi.org/10.1002/2016JB013765.

Farrell, W.E., 1972. Deformation of the Earth by surface loads. Rev. Geophys. 10, 761–797.

Griffiths, J., Ray, J.R., 2013. Sub-daily alias and draconitic errors in the IGS orbits. GPS Solut. 17 (3), 413–422. https://doi.org/10.1007/s10291-012-0289-1.

Gualandi, A., Serpelloni, E., Belardinelli, M.E., 2016. Blind source separation problem in GPS time series. J. Geod. 90 (4), 323–341. https://doi.org/10.1007/s00190-015-0875-4.

Gualandi, A., Avouac, J.P., Galetzka, J., et al., 2017. Pre- and post-seismic deformation related to the 2015, Mw7.8 Gorkha earthquake, Nepal. Tectonophysics 714–715, 90–106. https://doi.org/10.1016/j.tecto.2016.06.014.

Gualandi, A., Liu, Z., Rollins, C., 2020. Post-large earthquake seismic activities mediated by aseismic deformation processes. Earth Planet. Sci. Lett. 530. https://doi.org/10.1016/j.epsl.2019.115870 115870.

Hao, M., Freymueller, J.T., Wang, Q., et al., 2016. Vertical crustal movement around the Southeastern Tibetan Plateau constrained by GPS and GRACE data. Earth Planet. Sci. Lett. 437, 1–8. https://doi.org/10.1016/j.epsl.2015.12.038.

Hyvärinen, A., Oja, E., 2000. Independent component analysis: algorithms and applications. Neural Networks 13 (4–5), 411–430.

Jiang, W., Yuan, P., Chen, H., et al., 2017. Annual variations of monsoon and drought detected by GPS: A case study in Yunnan, China. Scientific Rep. 7 (1), 1–10.

Jiang, Z., Hsu, Y.J., Yuan, L., et al., 2021. Monitoring time-varying terrestrial water storage changes using daily GNSS measurements in Yunnan, southwest China. Remote Sens. Environ. 254 112249.

Larochelle, S., Gualandi, A., Chanard, K., et al., 2018. Identification and extraction of seasonal geodetic signals due to surface load variations. J. Geophys. Res.: Solid Earth 123 (12). https://doi.org/10.1029/2018JB016607.

Li, Z., Jiang, W., Liu, H., et al., 2012. Noise Model establishment and analysis of IGS reference station coordinate time series inside China. Acta Geodaetica et Cartographica Sinica 41 (1), 496–503.

Liu, B., Dai, W., Peng, W., et al., 2015. Spatiotemporal analysis of GPS time series in vertical direction using independent component analysis. Earth Planets Space 67 (1), 1–10. https://doi.org/10.1186/s40623-015-0357-1.

Liu, B., Dai, W., Liu, N., 2017. Extracting seasonal deformations of the Nepal Himalaya region from vertical GPS position time series using Independent Component Analysis. Adv. Space Res. 60 (12), 2910–2917. https://doi.org/10.1016/j.asr.2017.02.028.

Liu, B., King, M., Dai, W., 2018. Common mode error in Antarctic GPS coordinate time-series on its effect on bedrock-uplift estimates. Geophys. J. Int. 214 (3), 1652–1664. https://doi.org/10.1093/GJI/GGY217.

Mao, A., Harrison, C.G., Dixon, T.H., 1999. Noise in GPS coordinate time series. J. Geophys. Res. Solid Earth 104 (B2), 2797–2816.

Ming, F., Yang, Y., Zeng, A., et al., 2017. Spatiotemporal filtering for regional GPS network in China using independent component analysis. J. Geod. 91 (4), 419–440. https://doi.org/10.1007/s00190-016-0973-y.

Press W.H., Teukolsky S.A., Vetterling W.T., et al., 2001. Numerical recipes in Fortran 77: the art of scientific computing (2nd edn). Vol. 1 of Fortran numerical recipes, Cambridge University Press, Cambridge, pp 569–577.

Ray, J., Altamimi, Z., Collilieux, X., et al., 2008. Anomalous harmonics in the spectra of GPS position estimates. GPS Solut. 12 (1), 55–64. https://doi.org/10.1007/s10291-007-0067-7.

Ray, J., Griffiths, J., Collilieux, X., et al., 2013. Subseasonal GNSS positioning errors. Geophys. Res. Lett. 40 (22), 5854–5860. https://doi.org/10.1002/2013GL058160.

Rodell, M., Houser, P.R., Jambor, U., et al., 2004. The global land data assimilation system. Bull. Amer. Meteor. Soc. 85 (3), 381–394. https://doi.org/10.1175/BAMS-85-3-381 ISSN: 0003-0007, 1520-0477.

Rodriguez-Solano, C.J., Hugentobler, U., Steigenberger, P., et al., 2014. Reducing the draconitic errors in GNSS geodetic products. J. Geod. 88 (6), 559–574. https://doi.org/10.1007/s00190-014-0704-1.

Tan, W., Xu, X., Dong, D., et al., 2017. Themoelastic Seasonal Deformation in Chinese Mainland. Acta Geodaetica et Cartographica Sinica 46 (9), 1080–1087.

Tan, W., Chen, J., Dong, D., et al., 2020. Analysis of the potential contributors to common mode error in Chuandian region of China. Remote Sensing 1–11. https://doi.org/10.3390/rs12050751.

Yan, J., Dong, D., Bürgmann, R., et al., 2019. Separation of sources of seasonal uplift in China using independent component analysis of GNSS time series. J. Geophys. Res.: Solid Earth, 1–21.https://doi.org/10.1029/2019JB018139.

Yuan, P., Jiang, W., Wang, K., et al., 2018a. Effects of spatiotemporal filtering on the periodic signals and noise in the GPS position time series of the Crustal Movement Observation Network of China. Remote Sens., 10(9), 1472.

Yuan, P., Li, Z., Jiang, W., et al., 2018b. Influences of environmental loading corrections on the nonlinear variations and velocity uncertainties for the reprocessed global positioning system height time series of the crustal movement observation network of China. Remote Sens., 10(6), 958.

Zhang, J., Bock, Y., Johnson, H., et al., 1997. Southern California permanent GPS geodetic array: error analysis of daily position estimates and site velocities. J. Geophys. Res. Solid Earth 102 (B8), 18035–18055.

Zhan, W., Li, F., Hao, W., et al., 2017. Regional characteristics and influencing factors of seasonal vertical crustal motions in Yunnan, China. Geophys. J. Int. 210 (3), 1295–1304. https://doi.org/10.1093/gji/ggx246.

Zajdel, R., Sośnica, K., Bury, G., et al., 2020. System-specific systematic errors in earth rotation parameters derived from GPS, GLONASS, and Galileo. GPS Solut. 24 (3). https://doi.org/10.1007/s10291-020-00989-w.